Engineerable femtosecond pulse shaping by second-harmonic generation with Fourier synthetic quasi-phase-matching gratings

G. Imeshev

E. L. Ginzton Laboratory, Stanford University, Stanford, California 94305

A. Galvanauskas and D. Harter

IMRA America, 1044 Woodridge Avenue, Ann Arbor, Michigan 48105

M. A. Arbore, M. Proctor, and M. M. Fejer

E. L. Ginzton Laboratory, Stanford University, Stanford, California 94305

We describe a pulse-shaping technique that uses second-harmonic generation with Fourier synthetic quasi-phase-matching gratings. We demonstrate both amplitude and phase tailoring by generating a picosecond squarelike pulse as well as trains of femtosecond pulses with a terahertz-range repetition rate from either a compressed or a chirped pump pulse.   © 1998 Optical Society of America

OCIS codes: 320.5540, 070.2580, 050.2770, 320.2550.

Manipulation of the temporal shape of ultrashort optical pulses is important for many applications, such as communications, remote sensing, signal processing, and spectroscopy. Conventional pulse-shaping techniques use filtering of optical frequency components that are spatially dispersed with a grating apparatus.[1] Here we propose an alternative approach to pulse shaping that uses second-harmonic generation (SHG) with Fourier synthetic quasi-phase-matching (QPM) gratings. These monolithic and compact devices allow generation of almost arbitrary second-harmonic (SH) waveforms, because the lithographically defined nature of the structure intrinsically allows engineering of its amplitude and phase response.

The utility of Fourier synthetic QPM gratings for generation of arbitrary SH waveforms can best be understood in the frequency domain. For plane-wave QPM SHG, when we neglect pump depletion and the intrapulse group-velocity dispersion (GVD), the Fourier transform of the output SH pulse, $\widehat{A_2}(\Omega)$, is related to the Fourier transform of the square of the first-harmonic (FH) pulse, $\widehat{A_1^2}(\Omega)$, through the simple transfer-function relation[2]

$$\widehat{A_2}(\Omega) = \hat{D}(\Omega)\widehat{A_1^2}(\Omega), \qquad (1)$$

where $\Omega = \omega - \omega_n$ is the detuning of the angular frequency from the spectral centers of the FH ($\omega_n = \omega_1$) and the SH ($\omega_n = \omega_2 = 2\omega_1$) pulses. $\hat{D}(\Omega)$ is the QPM transfer function related to the spatially modulated nonlinear coefficient, $d(z)$, by the Fourier transform

$$\hat{D}(\Omega) = \Gamma \int_{-\infty}^{\infty} \mathrm{d}(z')\exp[i(\Delta k_0 + \Omega\,\delta\nu)z']\mathrm{d}z', \qquad (2)$$

with $\Gamma = -i\pi/\lambda_1 n_2$. The group-velocity mismatch (GVM) parameter is $\delta\nu = 1/u_1 - 1/u_2$, where u_1 and u_2 are the group velocities of the FH and the SH, respectively. The k-vector mismatch is $\Delta k_0 = 4\pi(n_2 -$ $n_1)/\lambda_1$, where the refractive indices n_1 and n_2 are evaluated at the center frequencies for FH and SH pulses, respectively, and λ_1 is the center wavelength of the FH pulse.

Given the temporal shape of the FH pulse, we can obtain the desired shape of the SH pulse by choosing $d(z)$ as an inverse Fourier transform of the desired transfer function $\hat{D}(\Omega)$. The pertinent Fourier component of the grating, $d_m(z)$, can be represented in the most general form as

$$d_m(z) = |d_m(z)|\exp[-iK_m z - i\Phi(z)], \qquad (3)$$

where we explicitly factored out the linear component of the total phase of the grating, $K_m z$, because for efficient mth-order QPM SHG with a uniform grating [$\Phi(z) \equiv 0$] the condition $K_m = \Delta k_0$ must be satisfied.[3] We can obtain any desired phase of the grating, $\Phi(z)$, beyond the $K_m z$ component, by choosing the local k vector of the grating, $K(z)$, as $K(z) = K_m + \mathrm{d}\Phi/\mathrm{d}z$. $|d_m(z)|$ in Eq. (3) is the amplitude of the mth Fourier component of the grating, so we can achieve a continuous modulation of $|d_m(z)|$ by varying the local duty cycle of the grating, $G(z)$. For a square grating,[3] $|d_m(z)| = (2/\pi m)d_{\mathrm{eff}}\sin[\pi m G(z)]$, where d_{eff} is the material's intrinsic nonlinear coefficient. If $G = 0$, i.e., the material is unmodulated, then $|d_m| = 0$, indicating that there is no modulated component of the QPM grating. The maximum value of $|d_m|$ is $(2/\pi m)d_{\mathrm{eff}}$ and is achieved at $G = 0.5$ for an odd-order or at $G = 0.25$ for an even-order QPM process.

In the time domain, pulse shaping with Fourier synthetic QPM gratings can be explained by the combination of the group-velocity walk-off effect and the spatial localization of the SHG process.[2] A particular frequency component of the FH generates a corresponding SH frequency component at spatial positions at which SHG is phase matched. Because of the GVM this SH frequency component undergoes a particular time delay relative to the FH pulse, as observed at

the output of the grating. This time delay is determined by the GVM parameter $\delta\nu$ and the spatial position at which the SH is generated; the former is a material property, whereas the latter is defined by the grating design.

The Fourier synthetic QPM gratings were fabricated in a single 25-mm-long chip from a 0.5-mm-thick LiNbO$_3$ wafer by the electric-field poling technique.[4] All devices were designed for first-order QPM ($m = 1$) and used binary modulation of the amplitude of the gratings, i.e., the local duty cycle was either $G = 0$ or $G = 0.5$, corresponding to $|d| = 0$ or $|d| = (2/\pi)d_{\text{eff}}$, respectively. We self-phase modulated output pulses from an amplified Er:fiber laser to produce 2.5-nJ pulses with 22-nm-wide spectra at 1560 nm. These pulses were compressible in a diffraction-grating compressor to 250 fs FWHM, with a resulting time–bandwidth product that was 1.6 times above the bandwidth limit. The pump beam was loosely focused through the sample to a spot with a $1/e$ electric-field radius of 85 μm.

As an example of Fourier synthetic QPM shapers, we demonstrated three devices, labeled (a), (b), and (c) in Fig. 1. Device (a) was simply a uniform grating for which we chose the QPM period $\Lambda_0 = 19$ μm to achieve phase matching at 98 °C when the device was pumped at 1560 nm. The length of this device, $L = 25$ mm, was much longer than the group-velocity walk-off length, L_{gr}, which is defined as the distance at which the SH pulse becomes delayed with respect to the transform-limited FH pulse by its initial pulse length τ_0; $L_{\text{gr}} = \tau_0/\delta\nu$. For SHG of a 1560-nm FH in LiNbO$_3$, $\delta\nu = 0.30$ ps/mm, and hence $L_{\text{gr}} = 0.8$ mm for 250-fs pulses. SH autocorrelation trace (a) in Fig. 2 has a triangular profile, which implies that the pulse has a squarelike shape. The FWHM of the trace is 7.4 ps, in agreement with the expected pulse length $\delta\nu L = 7.5$ ps.

Device (b) consisted of 13 uniform grating segments of length $L_s = 0.5$ mm with a QPM period of $\Lambda_0 = 19$ μm, alternating with segments of unmodulated material of length $L_u = 1.5$ mm. Because by design $L_s < L_{\text{gr}} < L_u$, each segment generated a short transform-limited SH pulse, and these pulses did not overlap temporally at the output. Autocorrelation trace (b) in Fig. 2 consists of 25 pulses with an interpulse separation of 0.59 ps and has a triangular envelope. Thus the underlying SH waveform has 13 uniformly spaced pulses of equal amplitude with a repetition rate of 1.69 THz. This result agrees with the expected spacing between peaks of adjacent pulses $\delta\nu(L_s + L_u) = 0.60$ ps. The individual pulses in the train are 210 fs long, as estimated with a numerically calculated deconvolution factor 0.77.

Device (c) consisted of five identical chirped grating segments of length $L_s = 5$ mm with no gap of unmodulated material between them. The QPM period of each segment varied linearly from 18.6 to 19.4 μm. Different spectral components of the chirped pump pulse were frequency doubled at different locations along each chirped segment, and hence the corresponding SH frequency components experienced different delays relative to the FH pulse. We chose the chirp of the

FH pulse to match the chirp of the grating segment, resulting in a compressed SH pulse.[2] Autocorrelation trace (c) in Fig. 2 indicates the train of five pulses with a repetition rate of 0.67 THz and separation between peaks of 1.49 ns, in agreement with $\delta\nu L_s = 1.50$ ps. Individual pulses in the train are 190 fs long, as we determined by using the same deconvolution factor as in device (b).

The spectra of the shaped SH pulses are shown in traces (a)–(c) of Fig. 3. For comparison we also include the spectrum obtained with a single short uniform grating segment of length 0.5 mm (b); see trace (d). The acceptance bandwidth of this device is broader than the bandwidth of the pump pulse, so the SH spectrum is proportional to the Fourier transform of the square of the FH pulse. Thus trace (d) indicates the maximum bandwidth available for the SH, whereas shaped pulses (a)–(c) reveal spectral filtering associated with pulse shaping.

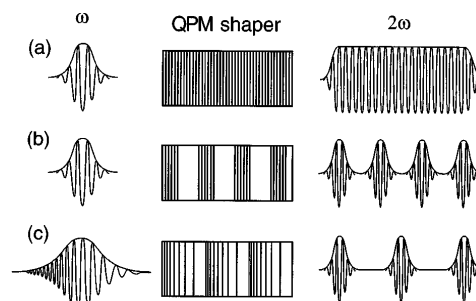The SH spectrum obtained with device (a) shows a single narrow peak, consistent with the long SH pulse

Fig. 1. Schematics of the pulse-shaping devices used in experiment: (a) a long uniform grating for generation of a transform-limited picosecond SH pulse, (b) uniform grating segments separated by unmodulated material for generation of a train of femtosecond transform-limited pulses; devices (a) and (b) are pumped by a transform-limited femtosecond FH pulse; (c) chirped grating segments for generation of a train of transform-limited femtosecond SH pulses from a chirped FH pulse.
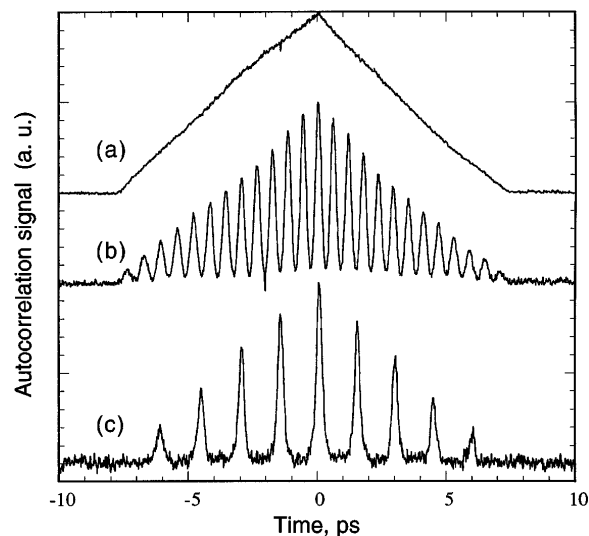

Fig. 2. Autocorrelation traces of the shaped SH pulses. Traces (a), (b), and (c) correspond to devices (a), (b), and (c) of Fig. 1.
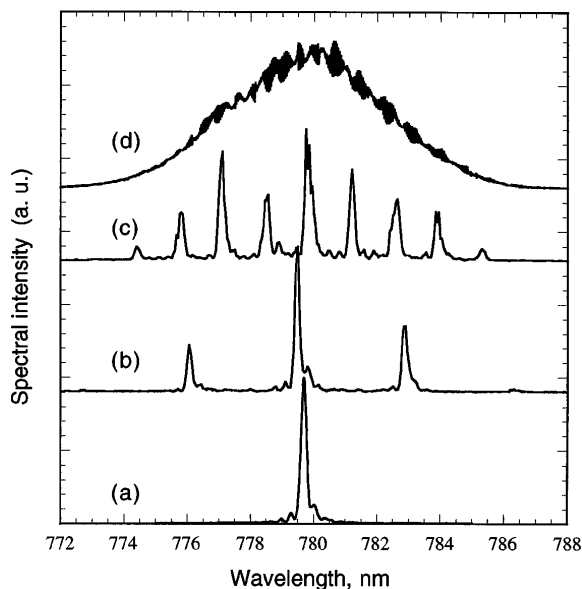
Fig. 3. Spectra of the shaped pulses: Traces (a), (b), and (c) correspond to traces (a), (b), and (c) of Fig. 2. Spectrum (d) was obtained with a single uniform gating segment whose acceptance bandwidth was broader than the bandwidth of the pump pulse.

that was obtained. Spectra obtained with devices (b) and (c) consist of several narrow peaks separated by 3.4 and 1.43 nm, respectively. From the temporal separation between pulses [0.59 ps for device (b) and 1.50 ps for device (c)], we find that the spectral spacing should be 3.4 and 1.36 nm, respectively, in agreement with directly measured values. It should be noted here that relative phases of the generated SH pulses are defined by the relative phases of the grating segments. Devices (b) and (c) were designed such that the adjacent grating segments are offset by exactly 2.000 and 5.000 mm, respectively, which are not the integral number of $\Lambda_0 = 19$ μm. Therefore the SH pulses in the trains have different phases and the spectra [traces (b) and (c) in Fig. 3] consist of narrow peaks whose amplitudes do not follow the envelope outlined by trace (d). Our calculations show that the pulse trains with relative pulse phases as obtained from the exact positions of the grating segments give spectral amplitudes that are consistent with traces (b) and (c). To generate SH pulses with specified relative phases, such as identical phases, one must use an appropriate grating design with fine positioning of the segments within Λ_0. This is no more difficult to implement lithographically than the patterns demonstrated here.

The efficiency scaling for QPM shapers is a complicated function of focusing, spectra, and the particular shaping function. For the special case of confocal focusing, a transform-limited FH pulse, and a binary-modulated (with duty cycle Q) uniform grating [e.g., devices (a) and (b)] the efficiency normalized to that of a device one walk-off length long [=95%/nJ for SHG of 1.56-μm FH in LiNbO$_3$ (Ref. 5)] equals Q. The observed efficiency of $\approx 5\%$ for device (b), corrected for focusing that is looser than confocal, corresponds to this scaling.

The shortest SH temporal feature that can be obtained, δt, is inversely related to the total bandwidth Δf that is available from the FH pulse, $\delta t \propto 1/\Delta f$, where the proportionality constant is of the order of unity and its exact value depends on the shape of the pulses. The maximum possible temporal window T (or the best spectral resolution $\delta f \propto 1/T$) of the shaper is determined by the length L of the device, $T = \delta \nu L$.

The intrapulse GVD effect was neglected in the present analysis. Under the conditions of this experiment this is a valid approximation, because the characteristic lengths at which GVD becomes important, $L_{\mathrm{GVD}}^{(i)} = \tau_0{}^2/|\xi_2^{(i)}|$, where $\xi_2^{(i)}$ is the GVD parameter for the FH ($i = 1$) and the SH ($i = 2$), are $L_{\mathrm{GVD}}^{(1)} = 670$ mm and $L_{\mathrm{GVD}}^{(2)} = 360$ mm; these values are large compared with the length of the devices (25 mm). Our preliminary studies indicate that GVD at the SH cannot be neglected when $\xi_2^{(2)}\Omega$ for frequencies within the bandwidth of the SH pulse becomes comparable with the GVM parameter $\delta \nu$. For pulses longer than ≈ 50 fs no compensation for the GVD would be necessary. For pulses with $\delta t \geq 10$ fs GVD at the SH could straightforwardly be accounted for in the design of the QPM shaper by appropriate choice of the k vector and (or) the duty cycle of the grating. Correct inclusion of GVD at the FH is a subject of current research.

In conclusion, we have demonstrated a femtosecond pulse-shaping technique that relies on the engineerability of the phase and amplitude response of QPM gratings. Fourier synthetic QPM gratings combine pulse shaping and SHG in a single monolithic and compact device that does not require critical alignment. This method could be applied to a variety of more-complex pulse-shaping functions, such as those that were demonstrated with conventional shaping techniques.[1] Extension of this technique to a shorter wavelength range that is accessible with Ti:Al$_2$O$_3$ lasers would require shorter QPM periods (≈ 2.5 μm) and raise concerns about two-photon absorption in LiNbO$_3$, which suggests that LiTaO$_3$ might be a better candidate for a Ti:Al$_2$O$_3$-pumped pulse shaper.

References

1. A. M. Weiner, Prog. Quantum Electron. **19,** 161 (1995).
2. M. A. Arbore, O. Marco, and M. M. Fejer, Opt. Lett. **22,** 865 (1997); M. A. Arbore, A. Galvanauskas, D. Harter, M. H. Chou, and M. M. Fejer, Opt. Lett. **22,** 1341 (1997).
3. M. M. Fejer, G. A. Magel, D. H. Jundt, and R. L. Byer, IEEE J. Quantum Electron. **28,** 2631 (1992).
4. L. E. Myers, R. C. Eckardt, M. M. Fejer, R. L. Byer, W. R. Bosenberg, and J. W. Pierce, J. Opt. Soc. Am. B **12,** 2102 (1995).
5. M. A. Arbore, M. M. Fejer, M. E. Fermann, A. Hariharan, A. Galvanauskas, and D. Harter, Opt. Lett. **22,** 13 (1997).